First Principles Modeling of Tritium Trapping in γ-LiAlO₂ Nanovoids

September 2020

Michel Sassi
Arun Devaraj
Steven R. Spurgeon
Bethany E. Matthews
David J. Senor

DISCLAIMER

This report was prepared as an account of work sponsored by an agency of the United States Government. Neither the United States Government nor any agency thereof, nor Battelle Memorial Institute, nor any of their employees, **makes any warranty, express or implied, or assumes any legal liability or responsibility for the accuracy, completeness, or usefulness of any information, apparatus, product, or process disclosed, or represents that its use would not infringe privately owned rights**. Reference herein to any specific commercial product, process, or service by trade name, trademark, manufacturer, or otherwise does not necessarily constitute or imply its endorsement, recommendation, or favoring by the United States Government or any agency thereof, or Battelle Memorial Institute. The views and opinions of authors expressed herein do not necessarily state or reflect those of the United States Government or any agency thereof.

PACIFIC NORTHWEST NATIONAL LABORATORY
operated by
BATTELLE
for the
UNITED STATES DEPARTMENT OF ENERGY
under Contract DE-AC05-76RL01830

Printed in the United States of America

Available to DOE and DOE contractors from
the Office of Scientific and Technical
Information,
P.O. Box 62, Oak Ridge, TN 37831-0062
www.osti.gov
ph: (865) 576-8401
fox: (865) 576-5728
email: reports@osti.gov

Available to the public from the National Technical Information Service
5301 Shawnee Rd., Alexandria, VA 22312
ph: (800) 553-NTIS (6847)
or (703) 605-6000
email: info@ntis.gov
Online ordering: http://www.ntis.gov

First Principles Modeling of Tritium Trapping in γ-LiAlO₂ Nanovoids

September 2020

Michel Sassi
Arun Devaraj
Steven R. Spurgeon
Bethany E. Matthews
David J. Senor

Pacific Northwest National Laboratory
Richland, Washington 99354

Abstract

Experimental STEM and APT investigations both indicate the presence of nanovoids in γ-LiAlO$_2$ pellets. While those nanovoids can affect the diffusion of tritium in pellets, first principles simulations have been conducted to evaluate the potential for tritium trapping by single and double cation and anion vacancies. It was found that tritium trapping allows recovery of a significant amount of the formation energy cost of cation vacancy, while the trapping of tritium by anion vacancies further increase the energy cost of forming a vacancy. The simulations also indicated the potential for tritium to be trapped in various forms by forming bonds such as Al—T, O—T or T$_2$. These results raise further questions regarding the speciation and dynamics of tritium trapped in nanovoids.

1.0 Introduction

In the design of the tritium-producing burnable absorber rods (TPBAR), the essential components for tritium production are the γ-LiAlO$_2$ pellets, which contain about 25% of the total lithium as ^{6}Li. Despite a total Li burnup of about 12% (i.e. ~50% of total ^{6}Li), the LiAlO$_2$ pellets can survive very well neutron irradiation during the 18 months of in-reactor operation.[1] In order to improve the fundamental understanding of physical phenomena occurring in TPBARs during irradiation, a series of post-irradiation examinations were conducted for the various components of the TPBAR. In the specific case of the pellets, several characterization techniques were used, such as scanning transmission electron microscopy (STEM) and atom probe tomography (APT), to identify irradiation induced microstructures at the nano- to micro-scale level.

In FY19, the project lead by Arun Devaraj[2] characterized by APT three TPBAR pellets from Cycle 13, labelled C13-2-2-2-P2, C13-3-5-2-P9, and C13-2-2-2-P14. Some key results of the APT analysis from each pellet were the detection of clusters of tritium and OT species in LiAlO$_2$ (Figure 1a, 1b), and the indication that both T and OT were heterogeneously distributed. In the density maps shown in Figures 1(c-f), high (red) and low (blue) density regions of T and OT, sometimes spatially separated, can be observed. While these observations provided valuable insights regarding the distribution and speciation of T in LiAlO$_2$ pellets, they also suggested that tritium can be trapped in LiAlO$_2$ nanovoids which sizes typically evolve around 5 nm or less.

In order to address knowledge gaps related to the evolution of the pellet microstructures during irradiation, which have implications on tritium diffusion, the work performed in this project uses a combination of APT, STEM, and first principles simulations to gather structural and chemical information on nanovoids and explore the defect energetics related to the formation of vacancy and vacancy clustering in γ-LiAlO$_2$. The potential for tritium trapping has also been computationally investigated. The results suggest that tritium can favorably be trapped in cation vacancies in various forms by forming bonds such as O—T or T$_2$.
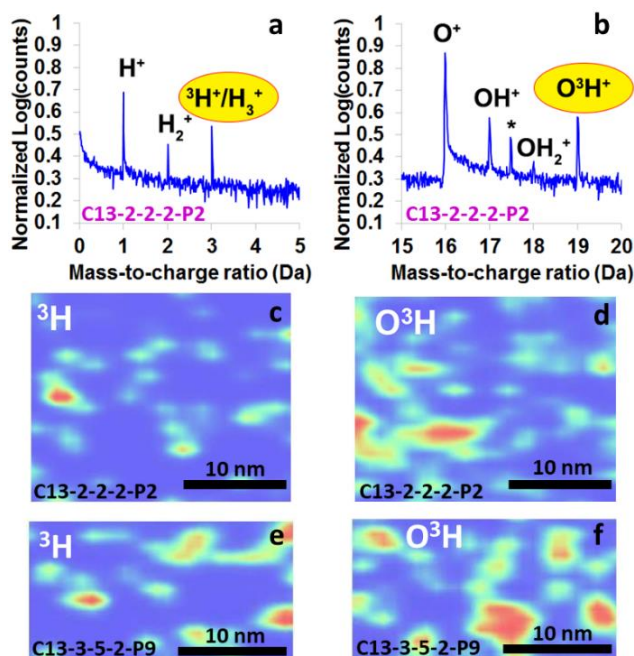
Figure 1. (a-b) APT mass-to-charge spectra highlighting detection and (c-f) heterogeneous distribution of T and OT species presumably in nanovoids in irradiated LiAlO$_2$ pellets from APT.

2.0   Experimental Investigations

2.1   Delays

Due to the restrictions of Laboratory access during the COVID-19 outbreak, the experimental APT and STEM works have been unfortunately delayed and only a portion of the work could be performed. Despite these circumstances, the section below summarizes some analysis that were carried out by STEM before Laboratory closure, from samples that were made in January 2020.

2.2   Sample preparation and imaging

In order to gather information about the structure of nanovoids and their environment, four APT pellets samples from C13-2-2-2-P8 cycle were lifted out and successfully transferred for scanning transmission electron microscope (STEM) imaging. A series of STEM analysis techniques were applied to each sample such as, high-angle annular dark-field (HAADF), medium angle annular dark field (MAADF), and bright field (BF) imaging, which are respectively sensitive to composition, strain, and phase contrast. Energy-dispersive X-ray spectroscopy (EDS) analysis has also been carried out to perform compositional characterization of the samples. Some of the images collected for each sample are shown in Figure 2. The images of Samples #1, #2, and #3 reveal complex microstructures with secondary phases and 10 – 20 nm nanovoids. Grain boundaries and inclusions are also present in the samples. Interestingly, the size of the nanovoids detected by STEM are larger than those observed in APT (see Figure 1), suggesting a range of size distribution for the nanovoids. In contrast, the images analysis of Sample #4, showed a much more uniform sample, with fewer defects present. Further quantification of nanovoid structures will require the preparation of separate, thinner STEM samples to perform focal series of imaging and electron energy loss spectroscopy (EELS) characterization of these complex microstructures.
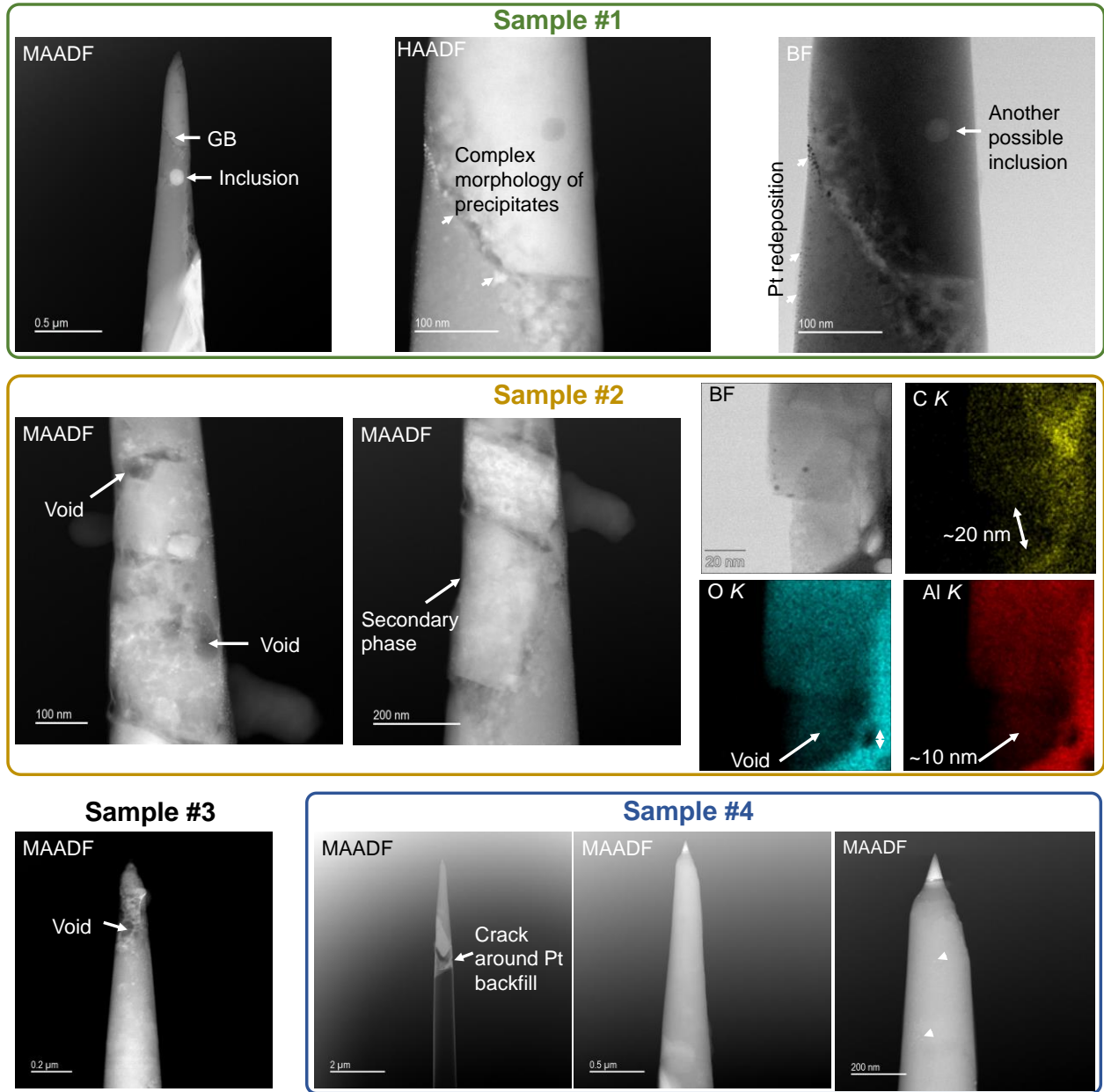
Figure 2. Some STEM images of four samples from C13-2-2-2-P8 showing a complex array of microstructures in neutron irradiated pellets.

3.0 Theoretical Investigations

3.1 Computational methods

First-principles simulations based on density functional theory (DFT) were carried out using the VASP package[3] to assess the formation energy of different types of defects and vacancy clustering, with and without tritium, in bulk γ-LiAlO$_2$. All the simulations used the generalized gradient approximation (GGA) exchange-correlation as parametrized in the Perdew, Burke, and Ernzerhof (PBE) functional.[4,5] Due to their similar electronic structure, the pseudo-potential of hydrogen has been used to describe tritium. To account for dispersive interactions between the tritium atom and its environment, van der Waals corrections as implemented in the Becke-Jonson damping method (DFT-D3) have been used.[6,7] All the calculations have been performed with spin-polarization and used a cutoff energy of 520 eV for the plane-wave basis set.[8]

Defect-free and defective supercells of γ-LiAlO$_2$ were generated to calculate the formation energy of cation and anion vacancies. A single vacancy was created in a supercell, resulting from the 2×2×2 multiplication of the primitive cell, while two vacancies were created in a 3×3×2 supercell. In each simulation, the atomic coordinates and lattice parameters were fully relaxed using a convergence criterion of 10^{-5} eV/cell for the total energy and 10^{-4} eV/Å for the force components. A Monkhorst-Pack[9] k-point mesh sampling of 5×5×4 and 3×3×4 were used for the 2×2×2 and 3×3×2 supercells respectively. The relaxed lattice parameters of the primitive cell were a=5.1634 Å (-0.11%), b=5.1634 Å (-0.11%), and c=6.2496 Å (-0.11%), which are in close agreement with the experimental parameters of a=5.1685 Å, b=5.1685 Å, and c=6.2565 Å.[10]

The temperature-dependence of the Gibbs free energy of defects has been determined by ab initio thermodynamics simulations. In these calculations, the Gibbs free energy of formation of defects, $\Delta G_f(T)$, has been calculated from the following generic equation:

$$\Delta G_f(T) = (\Delta\mu(0)_{SCD} + \Delta\mu(T)_{SCD}) + (\Delta\mu(0)_{RD} + \Delta\mu(T)_{RD}) - (\Delta\mu(0)_P + \Delta\mu(T)_P) \quad (1)$$

$$\Delta\mu(0) = E^{DFT} + E^{ZPE} \quad (2)$$

Where $\Delta\mu(0)_{SCD}$ and $\Delta\mu(T)_{SCD}$ are the chemical potentials of the defective supercell at 0 K and at T, $\Delta\mu(0)_{RD}$ and $\Delta\mu(T)_{RD}$ are the chemical potentials of the defect (removed atom) in its reference state at 0 K and at T respectively, $\Delta\mu(0)_P$ and $\Delta\mu(T)_P$ are the chemical potential of the perfect, defect-free supercell 0 K and at T respectively. For each case, the chemical potential at 0 K, $\Delta\mu(0)$, is the sum of the total DFT and zero-point energy. For the defective and perfect supercells of γ-LiAlO$_2$, the frequencies used to calculate the vibrational entropy contributions for the temperature-dependent chemical potential, $\Delta\mu(T)$, have been calculated using the Phonopy code.[11] The DFT total energies, E^{DFT}, of molecular O$_2$ and T$_2$ (assimilated to H$_2$) have been corrected to the experimental atomization energy of the gaseous species,[5] leading to an energy correction of -0.804 eV and -0.188 eV respectively. The temperature-dependent chemical potential, $\Delta\mu(T)$, for the reference states of bulk Al, bulk Li, O$_2$ and T$_2$ used the experimental values obtained from the NIST-JANAF thermochemical tables.[12]

3.2 Clustering of non-tritiated vacancies

In order to evaluate the potential for vacancy clustering in bulk γ-LiAlO$_2$, we have calculated the energy cost for creating single Li, Al, and O vacancies and compared it to the energy of two first neighbor vacancies. Table 1 shows that creating a single Al vacancy costs at least two times

more energy than creating a Li or O vacancy. However, as shown in Table 2, two Al vacancies interacting as first neighbor allow to reduce the energy cost of creating these vacancies by 12.47%.

Defect	E_F (eV)
V_{Li}	5.54
V_{Al}	13.03
V_O	6.86

Table 1. Single vacancy formation energy in bulk γ-LiAlO$_2$ calculated from DFT total energies.

In the list of vacancies combination investigated, Table 2 shows that vacancy clustering generally allows the system to reduce the energy cost of vacancy creation. Along with the interaction of two Al vacancies, the most important energy gains are obtained by the close interaction of Al and O vacancies, and Li and O vacancies, which would allow a 28.76% and 19.44% energy reduction respectively. In contrast, only a small energy gain, from 0.18% to 0.58%, is obtained when an Al and Li, two Li, or two O vacancies are interacting. The energy gain values, shown in Table 2, suggest that Li vacancies are strongly interacting with anion vacancies and not particularly interacting with cation vacancies (i.e. Al or other Li vacancies), while Al vacancies are strongly interacting with other Al vacancies and anion vacancies. In the case of oxygen vacancies, the clustering of anion-anion vacancies is not particularly favored in contrast to anion-cation vacancies.

Defect Pair	E_F (eV)		Relative energy gain (%)
	Isolated	*1st Neighbor*	
V_{Al}-V_{Al}	26.06	22.81	12.47
V_{Al}-V_{Li}	18.57	18.50	0.38
V_{Al}-V_O	19.89	14.17	28.76
V_{Li}-V_{Li}	11.08	11.06	0.18
V_{Li}-V_O	12.40	9.99	19.44
V_O-V_O	13.72	13.64	0.58

Table 2. Formation energy for two isolated and 1st neighbor interacting vacancies in bulk γ-LiAlO$_2$ calculated from DFT total energies. The relative energy gain from vacancy clustering is also provided.

3.3 Tritiation of isolated vacancies

The potential for tritium trapping by a single cation and anion vacancy has been investigated as function of the number of tritium atoms. As shown in Figure 3, up to four tritium atoms have been inserted in a single vacancy. In the case of Li vacancy, trapping one tritium atom by forming an O—T bond is the most energetically favorable configuration. This allows to reduce the cost of forming a Li vacancy by 47.47%. When two tritium atoms are trapped by the Li vacancy, the formation of a T_2 molecule is found to be energetically more favorable by 0.47 eV compared to forming two O—T bonds. While adding three tritium atoms still helps to reduce the energy cost of creating a Li vacancy, by forming one O—T bond and one T_2 molecule, the energy gain is less than when only one tritium is inserted. When four tritium atoms are inserted in the Li vacancy, it led to the formation on two O—T bonds and one T_2 molecule. However, the energy for creating a Li vacancy increases by 25.09%.
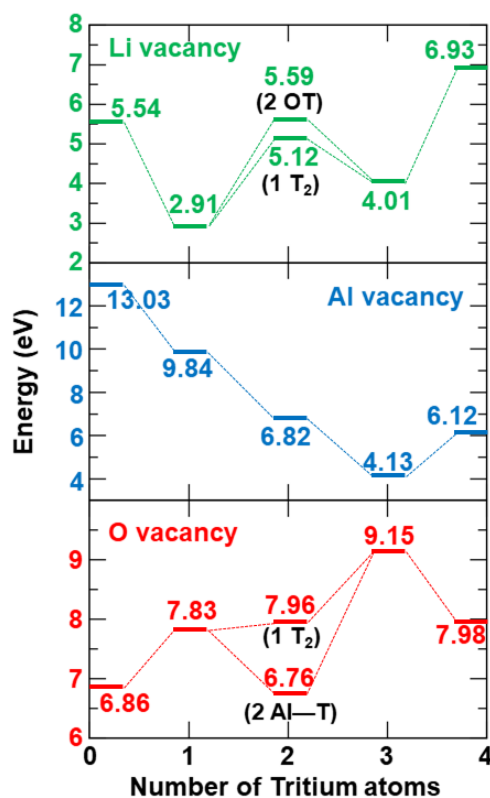
Figure 3. Variation of the creation energy of a single cation or anion vacancy as function of Tritiation.

In the case of Al vacancy, the addition of up to three tritium atoms gradually reduces the energy cost for creating a vacancy. For three tritium atoms, the energy gain is maximal with 68.3% of the energy cost recovered. For four tritium atoms, creating an Al vacancy is still favorable but

the energy gain is less important. Depending on the number of tritium atoms inserted in the Al vacancy, the formation of one to four O—T bonds are obtained. In contrast to the Li vacancy, no formation of T_2 species was obtained. The tritiation of the O vacancy is generally found to be energetically unfavorable, however, for two tritium atoms, the formation of two Al—T bonds is more favorable than forming one T_2 molecule. Forming two Al—T bonds is the only configuration, among those investigated, found to help reduce the energy cost of vacancy creation by 1.46%.

Altogether, the trends obtained for the tritiation of a single vacancy are consistent with the charge of the species removed to create the vacancy. For Li, Al and O vacancies, we found that inserting one, three and two tritium atoms respectively lead to the most energetically favorable configurations. Ultimately, all these configurations allow the system to reduce the cost of vacancy creation therefore suggesting that single cation, and to a lesser extent, anion vacancies can trap diffusing tritium atoms. The simulations conducted also highlight the potential for various tritium species to occur in the vacancy space, such as OT, AlT, and T_2. In the following, we use only the most energetically favorable tritium trapped configurations of each vacancy type to perform ab initio thermodynamic simulations.

3.4   Gibbs free energy of isolated vacancies with and without tritium

The temperature evolution of the Gibbs free energy of single vacancies with and without tritium has been determined from ab initio thermodynamics calculations. Figure 4 shows that for non-tritiated cation and anion vacancies, the Gibbs free energy of formation tends to decrease as the temperature increases. In the case of tritiated vacancy, a decrease of the Gibbs free energy is also obtained for Li and O vacancies but not for the tritiated Al vacancy which Gibbs free energy increases as the temperature increases. However, for both cation vacancies, tritiation helps to significantly reduce the energy cost of forming a vacancy at any temperature investigated. The range of temperatures at which TPBARs generally operate in reactor, between 563-623 K, has been highlighted in Figure 4 by a yellow band. At 600 K, the Gibbs free energy gain by tritiation of Li and Al vacancies is 44.74% and 58.55% respectively. In the case of the anion vacancy, tritiation is found to be always less favorable than a non-tritiated vacancy. While the Gibbs free energy of the O tritiated vacancy decreases as temperature increases, the extra energy cost at 600 K is 11.08%.

Even if the tritiation of O vacancy is not favorable, we note that at 600 K the extra cost in energy is about 0.65 eV, which is much smaller than the 2.32 eV and 7.19 eV energy gains from the tritiation of the Li and Al vacancies respectively. This observation suggests that tritium trapping in a nanovoid made of a mixture of both cation and anion vacancies should still be preferable. However, this preference would ultimately depend on several factors, such as the number of cation and anion removed to create the nanovoid, how much tritium are trapped, and the chemical form in which the tritium is trapped (e.g. AlT, OT, or T_2). It would also depend on the size, structure, and shape of the nanovoid. Some recent theoretical investigations of hydrogen trapping in nanovoids in oxides and metals found that the formation of OH groups in oxides could reduce the energy cost of forming cation vacancies,[13] while in metals, the formation of molecular H_2 could occur at the center of nanovoids.[14]
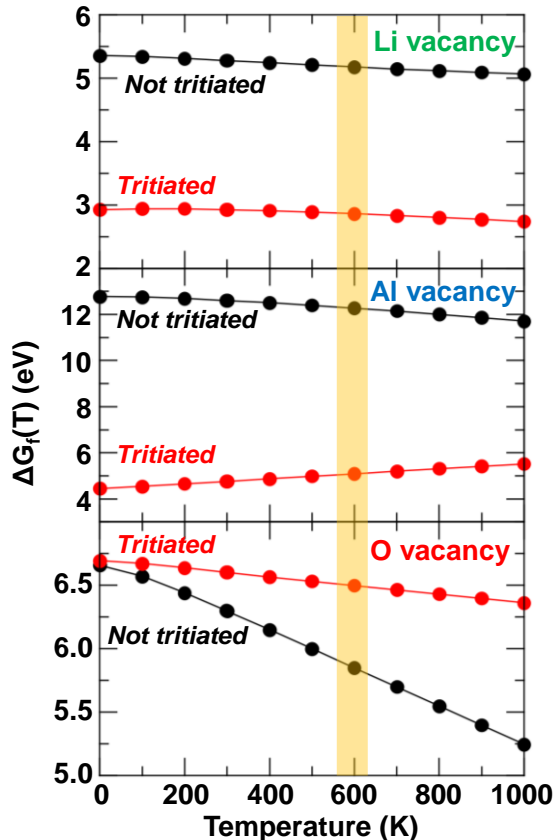
Figure 4. Variations of the Gibbs free energy, $\Delta G_f(T)$, as function of temperature for a single Li, Al and O vacancy without tritium and with one, three, and two tritium atoms respectively. The temperature zone highlighted in yellow represents the temperature range at which TPBARs operate in reactor.

3.5   Clustering of tritiated vacancies

In order to evaluate the energy gain from the aggregation of two tritiated vacancies, we used the most energetically favorable tritiation configurations found for a single vacancy as starting point for tritium addition in a cluster of two vacancies. This process led us to add one, three and two tritium atoms for each Li, Al and O vacancy created. For example, a cluster made of Li and O vacancies was filled with three tritium atoms, while a cluster of two interacting Al vacancies was filled with six tritium atoms. The formation energies calculated for two tritiated isolated and aggregated vacancies is shown in Table 3. For each combination investigated, the overall trend suggests that the clustering of tritiated vacancies generally allow an energy gain from 1.44% up to 8.16% compared to two isolated tritiated vacancies. While this result aligns with the results obtained previously for non-tritiated vacancies, it further suggests that a nanovoid formed by the clustering of cation and anion vacancies would act as a trap for diffusing tritium atoms. However, the diffusion and aggregation mechanisms of isolated tritiated vacancies remain unclear. While vacancies have the potential to trap tritium atoms, tritiated vacancies could diffuse slower which would limit the formation of nanovoids.

Defect Pair	E_F (eV)		Relative energy gain (%)
	Isolated	1st Neighbor	
V_{Al}-V_{Al}	8.26	7.85	4.99
V_{Al}-V_{Li}	7.04	6.94	1.44
V_{Al}-V_O	10.89	10.05	7.73
V_{Li}-V_{Li}	5.82	5.54	4.77
V_{Li}-V_O	9.67	8.88	8.16
V_O-V_O	13.53	12.98	4.04

Table 3. Formation energy for two tritiated isolated and 1st neighbor interacting vacancies in bulk γ-LiAlO$_2$ calculated from DFT total energies. The relative energy gain from vacancy clustering is also provided.

Conclusion

From experimental investigations, STEM image analysis revealed the presence of nanovoids from 10 to 20 nm size, along with a complex mix of microstructures such as secondary phases, cracks and grain boundaries. Further experimental investigations, correlating STEM and APT analysis are needed to extract more information about the size and distribution of nanovoid structures, as well as the speciation of tritium in those nanovoids.

The theoretical investigations conducted provide further evidences favorable to tritium trapping by small nanovoids. They also indicate the potential for tritium to be trapped in the vacancy space in various forms such as Al—T, O—T or T_2. Ab initio thermodynamics simulations suggest that tritium trapping by cation vacancies allows recovery of a significant amount of the cost of vacancy formation, while the trapping of tritium by anion vacancies further increases the energy cost of forming a vacancy.

Acknowledgments

This report was prepared as an account of work sponsored by an agency of the United States Government. Neither the United States Government nor any agency thereof, nor any of their employees, makes any warranty, express or implied, or assumes any legal liability or responsibility for the accuracy, completeness, or usefulness of any information, apparatus, product, or process disclosed, or represents that its use would not infringe privately owned rights. Reference herein to any specific commercial product, process, or service by trade name, trademark, manufacturer, or otherwise does not necessarily constitute or imply its endorsement, recommendation, or favoring by the United States Government or any agency thereof. The views and opinions of authors expressed herein do not necessarily state or reflect those of the United States Government or any agency hereof.

4.0 References

1 Senor, D.J. Science and technology in support of the tritium sustainment program. Report PNNL-27216 Rev. 1, Pacific Northwest National Laboratory (December 2018).

2 Devaraj, A.; Mathews, B.; Arey, B.; Sevigny, G. 3-D Mapping of Irradiation Dose Dependent Variation of Light Element Isotope Distribution in TPBAR Components by Atom Probe Tomography and Correlative Microscopy. Tritium Science Program project funded in FY19 (2019).

3 Kresse, G. and Furthmüller, J. Efficient iterative schemes for ab initio total-energy calculations using a plane-wave basis set. *Phys. Rev. B* **1996**, *54*, 11169-11186.

4 Perdew, J. P.; Burke, K.; Ernzerhof, M. Generalized Gradient Approximation Made Simple. *Phys. Rev. Lett.* **1996**, *77*, 3865−3868.

5 Perdew, J. P.; Burke, K.; Ernzerhof, M. Generalized Gradient Approximation Made Simple [Phys. Rev. Lett. 77, 3865 (1996)]. *Phys. Rev. Lett.* **1997**, *78*, 1396−1396.

6 Grimme, S.; Antony, J.; Ehrlich, S.; Krieg, H. A. Consistent and Accurate Ab Initio Parametrization of Density Functional Dispersion Correction (DFT-D) for the 94 Elements H-Pu. *J. Chem. Phys.* **2010**, *132*, 154104.

7 Grimme, S.; Ehrlich, S.; Goerigk, L. Effect of the damping function in dispersion corrected density functional theory. J. Comput. Chem. **2011**, *32*, 1456-1465.

8 Blöchl, P. E. Projector Augmented-Wave Method. *Phys. Rev. B: Condens. Matter Mater. Phys.* **1994**, *50*, 17953-17979.

9 Monkhorst, H. J.; Pack, J. D. Special points for Brillouin-zone integrations. *Phys. Rev. B* **1976**, *13*, 5188.

10 Wiedemann, D.; Indris, S.; Meven, M.; Pedersen, B.; Boysen, H.; Uecker, R.; Heitjans, P.; Lerch, M. Single-crystal neutron diffraction on γ-LiAlO$_2$: structure determination and estimation of lithium diffusion pathway. *Z. Krist-Cryst. Mater.* **2016**, *231*, 189-193.

11 Togo, A.; Tanaka, I. First principles phonon calculations in materials science. *Scr. Mater.* **2015**, *108*, 1-5.

12 *NIST-JANAF Thermochemical Tables*, 4th ed., edited by J. M. W. Chase American Chemical Society, Washington, DC, **1998**.

13 Luo, L. *et al.* Atomic origins of water-vapour-promoted alloy oxidation. *Nat. Mater.* **2018**, *17*, 514-518.

14 Hou, J.; Kong, X.-S.; Wu, X.; Song, J. Liu, C.S. Predictive model of hydrogen trapping and bubbling in nanovoids in bcc metals. *Nat. Mater.* **2019**, *18*, 833-839.

Pacific Northwest
National Laboratory

902 Battelle Boulevard
P.O. Box 999
Richland, WA 99354
1-888-375-PNNL (7665)

www.pnnl.gov